Role of mechanical forces in the stomach phase on the *in vitro* bioaccessibility of β-carotene

Tina A.J. Verrijssen[a], Maarten Vanierschot[b], Sofie I.M. Ongena[a], Ruth Cardinaels[c], Eric Van den Bulck[b], Ann M. Van Loey[a], Marc E. Hendrickx[a], Sandy Van Buggenhout[a]

[a] Laboratory of Food Technology and Leuven Food Science and Nutrition Research Centre (LFoRCe), Department of Microbial and Molecular Systems (M2S), KU Leuven, Kasteelpark Arenberg 22, PB 2457, 3001 Leuven, Belgium

[b] Department of Mechanical Engineering, KU Leuven, Celestijnenlaan 300A, PB 2421, 3001 Leuven, Belgium

[c] Soft Matter, Rheology and Technology (SMaRT), Department of Chemical Engineering, KU Leuven, Willem de Croylaan 46, PB 2423, 3001 Leuven, Belgium

Keywords: *in vitro* bioaccessibility, β-carotene, barriers, periodic forces, stomach-model, *in vitro* digestion

Abstract

The objective of this study was to examine the impact of flow conditions during the stomach phase of a simple *in vitro* digestion procedure on the microstructural properties and the β-carotene bioaccessibility of carrot-based model food systems containing oil and different barriers for β-carotene bioaccessibility. A 'periodic forces' stomach model, in which the flow characteristics (measured by Particle Image Velocimetry) corresponded well with experimental *in vivo* and *in silico* literature data, was successfully developed and implemented and used in a two-step static *in vitro* digestion procedure. This stomach model was compared with a conventional end-over-end rotation stomach model in which flow conditions were uncontrolled. Both models in combination with an end-over-end intestinal phase revealed differences in β-carotene bioaccessibility of carrot-based fractions due to the presence of different barriers (the plant chromoplast structure and/or the cell wall). Absolute β-carotene bioaccessibility values however differed between the models. The periodic forces stomach flow behavior lowered the β-carotene bioaccessibility in the β-carotene-enriched emulsion (72% versus 45%), the chromoplast fraction (66% versus 36%) and the large cell cluster fraction (22% versus 13%). The model also resulted in the presence of clusters of small oil droplets interspersed by surface-active compounds while large, coalesced oil droplets (D(v;0.9) of 189 μm) were observed after digestion in the end-over-end stomach model. As a consequence of the periodic forces stomach flow behavior also a slightly higher disintegration of carrot particles (to a D(v;0.9) of 450 μm instead of 492 μm) was observed which was however not linked to a higher β-carotene bioaccessibility in carrot cell clusters.

1 Introduction

Food industry has great interest in carotenoids because this group of fat-soluble bioactive compounds seems to have a positive impact on human health, including antioxidant capacity, pro-vitamin A activity and immune system enhancing properties (Dutta et al., 2005; Fernandez-Garcia et al., 2012). Since mammals need to obtain carotenoids from their diet, maximal absorption, or bioavailability of carotenoids from the food is desirable. Bioavailability is the fraction of the ingested carotenoids that is available for utilization in physiological functions and for storage in the body. It is partially determined by bioaccessibility, which is the fraction of the ingested carotenoids that is incorporated into micelles and thus becomes available for absorption in the body (Hedrén et al., 2002; Palafox-Carlos et al., 2011). Carotenoid bioaccessibility depends on several factors, such as the presence of oil and the matrix in which the carotenoids are embedded (Castenmiller & West, 1998; Hedrén et al., 2002). This is because on the one hand carotenoids are lipophilic molecules, and thus need to be incorporated in micelles before they can be absorbed and on the other hand because the localization of carotenoids within the plant structure is important. Carotenoids are located in chromoplasts, surrounded by a chromoplast membrane and situated in plant cells, which are in turn enclosed by a cell membrane and a cell wall (Jeffery et al., 2012). To investigate the bioaccessibility of carotenoids, different *in vitro* digestion models have been used (Lemmens et al., 2010; Courraud et al., 2013; Salvia-Trujillo et al., 2013). Within the stomach phase, it is however difficult to simulate the mechanical forces exactly as they occur *in vivo*. In most simple *in vitro* models, end-over-end rotations are used to mix the digest with stomach juice. The purpose of the present study is to control the mechanical forces (measured with Particle Image Velocimetry (PIV) and modeled with Computational Fluid Dynamics (CFD)) in a simple *in vitro* digestion model and to evaluate whether a more controlled way of applying mechanical forces in the *in vitro* stomach step would allow a more accurate simulation of *in vivo* stomach forces as reported in literature (Vassallo et al., 1992; Kamba et

al., 2000; Marciani et al., 2001a; Pal et al., 2004). Ferrua & Singh (2010) developped *in silico* a 3D stomach geometry. Their results corresponded well with results found using a 2D dimensional stomach model (Pal et al., 2004) and with *in vivo* anatomical data (measured with Magnetic Resonance Imaging (MRI)) (Marciani et al., 2001b; Ferrua & Singh, 2010). In the present work, the influence of mechanical forces in the stomach phase on β-carotene bioaccessibility was investigated. More particularly, it was the objective to compare the effect of uncontrolled *versus* controlled mixing during *in vitro* stomach digestion on the microstructural properties of plant-based food systems during digestion and on the resulting β-carotene bioaccessibility values. Thereto, the bioaccessibility of different carrot-based fractions was measured using two different *in vitro* digestion models that differed in the way mechanical forces in the stomach phase were applied (end-over-end rotation *versus* controlled up-and downward movement). Besides the bioaccessibility, oil droplet and particle size distributions of the digests were measured during the digestion to investigate on the one hand the effect of the mechanical forces on these sizes and on the other hand their effect on the β-carotene bioaccessibility. Because it is expected that the viscosity of the stomach content would influence the flow conditions (Marciani et al., 2001b), the viscosity of the stomach content was measured during the stomach phase.

2 Materials and methods

2.1 Materials

Fresh carrots (*Daucus carota* cv. Nerac) were purchased in a local shop in Belgium and stored at 4°C. Olive oil (extra virgin) was kindly donated by Vandemoortele (Ghent, Belgium). All chemicals and reagents were of analytical grade from Sigma Aldrich, except for NaCl, HCl, urea and ethanol (from VWR); $CaCl_2.2H_20$, NH_4Cl, $MgCl_2$ and $CaCl_2.2H_20$ (from Merck); hexane and acetone (from Chem Lab); glucose and $NaHCO_3$ (from Fisher Scientific); KCl (from MP Biomedicals).

2.2 Carrot-based fractions

2.2.1 β-carotene enriched oil-in-water emulsion

Carrot puree was prepared by mixing peeled carrot pieces and water (1:1) for 1 min in a kitchen blender (Waring Commercial, Torrington, CT, USA). Subsequently, this puree was homogenized (Panda 2K, Gea Niro Soavi, Parma, Italy) at 100 MPa using one cycle. Olive oil was enriched with β-carotene by rotating olive oil end-over-end with the homogenized carrot puree (1:5 w/w)for 5 hat room temperature. Afterwards, this mixture was centrifuged (at 4 °C during 15 min at 8739 g) (J2-HS centrifuge, Beckman, CA, USA) and the oil phase, enriched with β-carotene, was collected (Colle et al., 2010; Palmero et al., 2013). All enriched oil was prepared and stored shortly at -80°C until emulsions were prepared.

Aqueous emulsions containing 10% oil were prepared by blending (10 min) and homogenizing (100 MPa) the enriched oil phase with demineralized water in which 1% L-α-phosphatidylcholine was dissolved. Emulsions were prepared in duplicate. Each of them was independently submitted to the *in vitro* digestion procedure.

2.2.2 Chromoplast fraction

Peeled carrot pieces were mixed for 5 sec with a 0.05 % EDTA solution (1:1 w/w) in a blender (Waring Commercial, Torrington, CT, USA). This mixture was then filtered using a cheesecloth, after which the filtrate was centrifuged (J2-HS centrifuge, Beckman, CA, USA) at 27200g during 30 min (4°C). The pellet, which contains the chromoplasts, was dissolved in 100 ml deionized water (Palmero et al., 2013). The chromoplast fraction was prepared in duplicate. Each of them was independently submitted to the *in vitro* digestion procedure.

2.2.3 Small cell cluster fraction

Carrot puree was prepared by mixing peeled carrot pieces and water (1:1) for 2 min in a kitchen blender (Waring Commercial, Torrington, CT, USA). The small cell clusters were obtained by

collecting particles with sizes between 40 and 250 µm by wet sieving (Retsch AS200, Haan, Germany). The small cell cluster fraction was prepared in duplicate. Each of them was independently submitted to the *in vitro* digestion procedure.

2.2.4 Large cell cluster fraction

Carrot puree was prepared by mixing peeled carrot pieces and water (1:1) for 20 sec in a kitchen blender (Waring Commercial, Torrington, CT, USA). The large cell clusters were obtained by collecting particles with sizes between 800 and 2000 µm by wet sieving (Retsch AS200, Haan, Germany). The large cell cluster fraction was prepared in duplicate. Each of them was independently submitted to the *in vitro* digestion procedure.

2.3 *In vitro* digestion of carrot-based fractions

2.3.1 Preparation of the digests

Because of the fat-soluble character of carotenoids and the need of oil in the context of carotenoid bioaccessibility, a given amount (5 ml) of the oil-in-water emulsion was used for each digest. To obtain equal ratios of β-carotene concentration to lipid concentration in all digests, different amounts of water and carrot fraction were used to prepare the digests, as listed in Table 1. The oil-in-water emulsion was prepared by blending (10 min) and homogenizing (100 MPa) 10% of olive oil with demineralized water in which 1% of L-α-phosphatidylcholine was dissolved.

2.3.2 Digestion model

Digests were passed through a two-step static *in vitro* digestion model (Fig. 1). The applied biochemical conditions are described by Versantvoort et al. (2005), which means that stomach juice, duodenal juice and bile extract are composed according to the method of Versantvoort et al. (2005).

The mechanical conditions of the stomach phase are simulated by either an end-over-end rotation (Versantvoort et al*.,* 2005) or by controlled periodic forces, based on the method of Chen et al*.* (2011) with some modifications. As indicated in Fig. 1, the model with end-over-end rotations during the stomach phase as well as during the intestinal phase is called the "end-over-end digestion model", whereas the model with periodic forces during the stomach phase and end-over-end rotations during the small intestinal phase is called the "periodic forces digestion model". To minimize the influence of light and oxygen, the samples were kept in dark during the whole digestion procedure and the headspace of the tubes was flushed with nitrogen prior to each incubation step. The chemical and mechanical conditions applied to simulate the gastric and small intestinal phase of the digestion process are described in more detail in sections 2.3.2.1 and 2.3.2.2

2.3.2.1 Gastric phase

The first step in the digestion method is the simulation of the stomach phase by addition of stomach juice (pH 1.3), which contains mainly electrolytes, BSA, pepsin and mucin (Versantvoort et al., 2005) to the digest (Fig. 1). The mechanical conditions in the first model, namely end-over-end rotations, are uncontrolled. In the second model however, the mechanical conditions of the stomach phase are mimicked by applying an up- and downward movement along the x-direction of a spherical probe in a glass tube with a hemispherical bottom (Fig. 2a). The tube has an internal diameter D of 70 mm and an internal height H of 180 mm. The diameter of the spherical teflon probe D_p is 58 mm. This probe is connected to the load cell of a Texture Analyzer by a thin rod-shaped teflon adaptor (9 mm thick). The velocity of the probe, as a function of time, is shown in Fig. 2b. The maximum up (and down) ward velocity is 10 mm s^{-1}, giving a Reynolds number of the flow (based upon the probe diameter) ranging from 7.25 to 580 depending on the viscosity of the sample. As the probe moves up and down, the shear stresses in the flow field, taking into account the axisymmetry of the setup, are given by

$$\tau = \mu\left(\frac{\partial U}{\partial r} + \frac{\partial V}{\partial x}\right), \quad (1)$$

where U is the velocity component in the x-direction and V is the velocity component in the r-direction (radial direction). The shear rates in the flow field can be calculated by taking the ratio of the shear stress τ and the viscosity μ.

In order to determine the shear rates in the setup, both an experimental and a numerical study is performed to obtain the velocity field. Experimentally, the flow field is measured by Time-Resolved Particle Image Velocimetry (TR-PIV) measurements using sugar-water solutions with different sugar concentrations. These sugar-water solutions were used as translucent solutions having different viscosities in the range of the viscosity of the carrot-based fractions. In addition to these experiments, a numerical simulation is performed using the commercial Computational Fluid Dynamics (CFD) code Fluent. For those simulations, Newtonian behavior is assumed for all samples. The equations of motion (Navier-Stokes equations) are solved using a finite volume approach. Since the flow field is laminar, no turbulence model is used. The flow domain is discretized using a deformable grid and hence the motion of the probe is simulated by a moving boundary. Details on the experimental and numerical setup and on the validation of the numerical calculations can be found in Vanierschot et al. (2013).

2.3.2.2 Small intestinal phase

After the stomach phase, the intestinal phase is simulated by adding 12 ml duodenal juice, 6 ml bile juice and 2 ml 1 M bicarbonate per 15.5 ml initial digest, as indicated in Fig. 1, after which the mixture is rotated end-over-end for 2 h, as described by Versantvoort et al. (2005).

2.4 Analysis of the structural properties

2.4.1 Viscosity

Since the viscosity of the stomach content affects the flow behavior in this phase, the viscosity of the digests was measured immediately after stomach juice was added and after the stomach phase. Measurements were performed with a stress-controlled rheometer (MCR 501, Anton Paar, Graz, Austria) at 25 °C, whereby a six-bladed vane was used as geometry to avoid slip. To avoid the effect of loading history on the samples, a constant shear rate of 40 s^{-1} was applied for 60 sec, followed by a rest-period of 120 sec (shear rate of 0 s^{-1}). The viscosity was then measured by decreasing the shear rate linearly from 40 to 0.04 s^{-1}. Each shear rate was applied for 20 sec and it was verified that steady state viscosities were obtained in this way. Evaporation can be considered negligible due to the short duration of each test. All analyses were carried out in duplicate.

2.4.2 Particle size distribution

The particle size and particle size distribution of the samples (before digestion, after the stomach phase and after the small intestinal phase) were measured by laser diffraction (Beckman Coulter Inc, LS 13 320, Miami, Florida). Hereto, the sample was poured into a stirred tank, filled with deionized water. The sample was pumped into the measurement cell wherein the laser light (wavelength main illumination source: 750nm; wavelengths halogen light for Polarization Intensity Differential Scattering (PIDS): 450 nm, 600 nm, 900 nm) is scattered by the particles. The parameters D(v;0.1), D(v;0.5) and D(v;0.9) are reported. The relative width of the particle size distribution (spread) was calculated as:

$$\text{spread} = \frac{(D[v,0.9]-D[v,0.1])}{D[3,2]} \quad (2)$$

All analyses were carried out in duplicate.

Besides laser diffraction, microscopic pictures were taken to visualize the microstructure of the samples. This was done by using a light microscope (Olympus BX-41) equipped with an Olympus XC-50 digital camera (Olympus, Opticel Co. Ltd., Tokyo, Japan).

2.4.3 In vitro *β-Carotene bioaccessibility*

The *in vitro* β-carotene bioaccessibility ($\frac{B}{C}$) was calculated as the amount of β-carotene in the micelles after digestion (B) relative to the initial amount of β-carotene in the digest (C).

The concentration of β-carotene in the samples was determined according to the procedure described by Lemmens et al. (2010). An extraction solvent containing hexane, aceton, ethanol (50:25:25) and 0.1% buthylated hydroxytoluene (BHT) was used to extract the β-carotene fraction. Besides the extraction solvent, also $CaCl_2$ and ultrapure water were added to clearly separate the organic and the aqueous phase. The organic phase, containing the β-carotene, was taken and the absorption of β-carotene was measured by a spectrophotometric analysis at 450 nm (=λ_{max} for β-carotene in hexane). The amount of β-carotene was then calculated as:

$$\text{amount of } \beta - \text{carotene } \left(\frac{\mu g}{\text{g emulsion}}\right) = \frac{\text{A .V (ml)}.10^4}{\text{E}^{1\%}_{1\text{ cm}}.\text{m (g)}} \quad (3)$$

where A is the measured absorbance (at 450 nm), V is the volume of the extract (25 ml hexane), $E^{1\%}_{1\ cm}$ is the extinction coefficient (2560 $\frac{100\ ml}{g\ cm}$) and m is the mass of the emulsion (in g) (Hart & Scott, 1995).

All analyses were carried out in triplicate.

The micelle fraction was obtained using the two different static *in vitro* digestion models (Fig. 1). After the small intestinal phase, the micelle fraction was collected by ultracentrifugation (165 000 g, 1 h and 5 min, 4 °C) and the concentration of β-carotene in this fraction was determined according to the procedure described above. This concentration represents the concentration of β-carotene in the micelles after digestion. All analyses were carried out in triplicate.

2.4.4 Statistical analysis

Differences in mean relative β-carotene bioaccessibility were analyzed using one-way anova and the Tukey's Studentized Rand Post-hoc Test (Statistical Software Package SAS, version 9.2., Cary, N.C., U.S.A.). The level of significance was 95% ($P<0.05$).

3 Results and discussion

3.1 The viscosity of digests during *in vitro* stomach digestion

The results show that the viscosities of the enriched oil emulsion digest with stomach juice and the chromoplast digest with stomach juice are similar (results not shown). Probably, this can be explained by the limited amount of the chromoplast fraction and the size of the chromoplasts in the digest. To obtain the same carotenoid concentration among the different digests, only a small amount of the chromoplast fraction was added to the digest having a negligible effect on the viscosity, especially because the chromoplast fraction particles are very small (10 µm) (Table 2) and may thus have less effect on the resistance against flow as compared to the oil droplets (diameter of maximum 3 µm approximately) (Table 2). Comparing the viscosity of the different samples (Fig. 3) clarifies that the viscosity of the samples with cell clusters is higher than the viscosity of the samples without cell clusters. This effect can be explained by the fact that large particles (D(v; 0.5) of 259 µm and 1189 µm for small and large cell clusters respectively, Table 2) are present in a substantial amount in the digests containing cell clusters (Table 1), substantially affecting the digest viscosity. Non-Newtonian behavior was noticed for all samples. This result was expected since the rheological behavior of most plant-based products has been described as non-Newtonian because of possible structural modifications occurring during shear application to the products (Steffe, 1996).

Among the tested digests, dilatant behavior (shear thickening) was noticed for the enriched oil emulsion with stomach juice and the chromoplast digest with stomach juice, whereas pseudoplastic behavior (shear thinning) was noticed for the small and large cell cluster digests with stomach juices. Differences might be attributed to the effect of on the one hand the structure of the emulsions, and on the other hand the structure of the plant particles on the applied shear rate (Hofmann et al*.,* 1991; Liu & Pine, 1996; Bromberg & Barr, 2000; Jones et al*.,* 2003; Moelants et al*.,* 2013). The viscosity of the different digests was also measured after the stomach phase digestion (results not shown). These results showed that the stomach digestion had no effect on the viscosity of the samples.

3.2 Flow field during *in vitro* stomach digestion

3.2.1 Comparison of experimental and numerical flow fields

For validation of the numerical simulations, the numerically calculated flow field inside the *in vitro* setup is compared with the flow field obtained from PIV measurements using sugar-water solutions having viscosity values comparable to those of the carrot-based fractions. The flow field inside the setup, when the probe is on the maximal height (velocity 0 cm s^{-1}), is shown in Fig. 4. Fig. 4a and 4c show the flow field measured by PIV and Fig. 4b and 4d- show the numerically simulated flow field. In Fig. 4a and 4b, water is chosen as a working fluid with a dynamic viscosity of 1 mPa.s, resulting in a Reynolds number of 580. Inside the confinement, the wake behind the probe creates a pair of counter rotating vortices. Further downstream of the wake, a second pair of counter rotating vortices is created by the hemispherical bottom of the confinement. The position of the centers of these vortices corresponds very well between experiments and numerical simulations.

As the Reynolds number of the flow decreases (by using a higher viscosity fluid), the flow field inside the setup alters significantly. Fig. 4c and 4d show the velocity field for sugar water with a viscosity of 12 mPa.s. The position and movement of the probe is the same as in Fig. 4a and 4b. Also the velocity vectors have the same absolute size. The wake behind the probe is significantly enlarged as compared to the case with a less viscous fluid. As a result, the second vortex pair has disappeared, as the viscous forces become more dominant with increasing viscosity. Comparing Figs. 4a,b,c and d shows that the flow field near the hemispherical bottom of the *in vitro* setup becomes more uniform and as a result, the velocity gradients decrease. This is in agreement with the conclusion of Ferrua and Singh (2010), who also found that the formation and strength of flow circulations (eddies) are dependent of the viscosity. It should be mentioned here that the maximum velocity of water, predicted in the antropyloric region of the stomach, namely 2.8 cm s^{-1} (Ferrua and Singh, 2010), is comparable with the maximum velocity of water in our periodic forces stomach model, namely 3.0 cm s^{-1} (Vanierschot et al., 2013).

3.2.2 Shear rates in the in vitro *setup*

Based on the velocity fields obtained inside the simulated stomach, the shear stress and hence the shear rate can be calculated using equation 1. Fig. 5 shows the shear rates in the simulated stomach for fluids with different viscosities. For each viscosity, the shear rate is maximal in the smallest cross section between probe and confinement and slightly higher on the probe side as compared to the confinement side. For the low viscosity fluid, the maximum shear rate is around 30 s^{-1} and the minimal shear rate is around -40 s^{-1}. For the high viscosity fluids, the shear rate becomes independent upon viscosity and the maximal and minimal values are around 25 and -30 s^{-1} respectively. It should be noted here that the non-Newtonian behavior of the food digests might slightly alter the shear rate profiles in the stomach model. Nevertheless, as the probe is motion-controlled, the shear rate range and distribution discussed above is expected to provide a good estimate of the flow profile in the stomach model with food digests.

3.3 The particle size (distributions) of carrot-based fractions during *in vitro* digestion

The particle size distributions of the different fractions were measured (Table 2) and visualized by microscopy (Fig. 6). From these results, it can be concluded that the oil droplets of the (enriched) oil emulsion have an average diameter of 1.17 µm. The chromoplast fraction contains a broad range of particle sizes (spread of 24), with diameters ranging from 1.7 µm (D(v;0.1)) to 66.0 µm (D(v;0.9)). Based on the comparison between these chromoplast particle sizes, the size of different chromoplasts reported in literature (2-4 µm for sweet orange fruit chromoplasts (Zeng et al. 2011) and 15-48 µm length, 1-2 µm diameter for tomato fruit chromoplasts (Rosso, 1986)) and the microscopic observations (Fig. 6 b), it is suggested that clusters of chromoplastic material exist in the carrot-based chromoplast fraction. As the D(v;0.1)-value and the D(v; 0.5)-value of the small cell cluster fraction are respectively smaller and larger than the mean diameter of a carrot cell, which is approximately 125 µm (Lemmens et al., 2010), it is clear that this fraction contains mainly cell clusters, but also some (broken) cells will occur. This is also visible on the microscopic image (Fig. 6 d). The large cell cluster fraction has a D(v;0.1)-value of 714 µm and a D(v;0.5)-value of approximately

1189 µm. This means that in this fraction, only cell clusters occur. On the microscopic images (Fig. 6) it is visible that in this case β-carotene is embedded in a chromoplast, which in its turn is clearly surrounded by a cell wall (Fig. 6 c,d,e).

The evolution of the particle size distributions of the four fractions during digestion was investigated. In Fig. 7, the particle size distributions before digestion (Fig. 7 a, b), after the stomach phase (Fig. 7 c, d) and after the small intestinal phase (Fig. 7 e, f) are given for the enriched oil emulsion (Fig. 7 a, c, e) and for the small cell cluster fraction (Fig. 7 b, d, f). Also microscopic pictures were taken at different stages of the digestion (Fig. 8).

The results of oil droplet size distributions of the enriched oil-in-water emulsion digest showed that the oil droplet size was increased after the end-over-end rotation stomach phase as compared to the initial oil droplet size while this was not the case for the periodic forces model. In addition, visual comparison of the oil droplets after the end-over-end and the periodic forces stomach phase revealed a remarkable difference (Fig. 8). Whereas large, coalesced oil droplets were noticed after the end-over-end stomach phase, clusters of small oil droplets interspersed with surface active compounds, like proteins or mucin, were observed after the periodic forces stomach phase (Fig. 8). Based on this observation, it can be hypothesized that the competitive absorption and displacement processes (Michalski et al*.,* 2005; McClements et al*.,* 2009; Singh et al*.,* 2009) between L-α-phosphatidylcholine, which is initially on the surface of the oil droplets, and surface active compounds in the stomach juice are influenced by the different mixing processes in the stomach phase. The clusters of small oil droplets (interspersed with surface active compounds) did not show up in the particle size distributions from laser diffraction, probably due to the fact that these clusters may break down in the continuous water flow during the measurement procedure so that only the size of the oil droplets is measured.

After the small intestinal phase (Fig. 8 c, d), the oil droplet size distributions are more or less comparable between the two digestion models, although the oil droplets obtained from the end-

over-end digestion model are slightly larger. However, based on the data of the oil droplet size (distribution) after the stomach phase, it was expected that the oil droplet sizes would differ more after the small intestinal phase. It can be hypothesized that the oil droplet size is important for the lipid digestion but that the transit time was sufficiently long to rule out the area-dependency (McClements et al*.,* 2009). Another possible reason is that the surface active compounds on the surface of the oil droplets after the periodic forces stomach phase hinder the activity of lipase more than for oil droplets with less surface active compounds bound to their surface (Fig. 8) (Mun et al*.,* 2007). Finally, it has to be mentioned that the mixing in the small intestinal phase is mimicked by an end-over-end rotation, which may destroy the oil droplet clustering after the periodic forces stomach phase. The presence of large, coalesced oil droplets after the end-over-end rotation stomach phase, clusters of oil droplets with proteins and mucin after the periodic forces stomach phase and more or less comparable oil droplet sizes after the small intestinal phases were also found for the oil emulsion part in the microscopic pictures of the chromoplast, small and large cell cluster digests (results not shown). Note that the spread of the oil droplet sizes after the small intestinal phase (41 and 58 after end-over-end and periodic forces digestion model respectively) is larger as compared to the spread after the stomach phases (23 and 3 after end-over-end and periodic forces stomach phase respectively), but that the volume fraction of oil phase decreased. This might be caused by the fact that droplet coalescence is promoted by lipid digestion (McClements et al*.,* 2009; Sing et al*.,* 2009).

The (possible) changes in size of the chromoplasts were not visible on the particle size distributions from laser diffraction because the size of the chromoplasts (1.7 – 66.0 µm) is very similar to that of the oil droplets and oil droplet clusters. Microscopic images however showed that less chromoplast clusters occur after the stomach or small intestinal phase, for both the end-over-end and the periodic forces models (results not shown).

Comparing the plant particle size distributions of the small and large cell cluster digests after the different digestion models revealed that the plant particles experience stress due to the applied

periodic forces and slightly break down. Fig. 7 d shows a slight decrease in particle size of the small cell clusters after the periodic forces stomach phase. Also for the large cell clusters, the D(v;0.1), D(v;0.5) and D(v;0.9)-values were measured after the different stomach phases. Those values were respectively 591, 1137 and 1735 after the end-over-end rotation stomach phase and 549, 1124 and 1672 µm after the periodic forces stomach phase, indicating that the plant particles abrade slightly more during the periodic forces stomach phase.

3.4 The *in vitro* β-carotene bioaccessibility of carrot-based fractions

In Fig. 9, the *in vitro* β-carotene bioaccessibility values of the different digests are given, for both the end-over-end and the periodic forces digestion models. The β-carotene bioaccessibility of the digests with cell clusters (between approximately 13% and 25%) appeared to be significantly lower than that of digests without cell clusters (between approximately 36% and 72%), in particular after the end-over-end digestion model (approximately 20-22% for the digests with cell clusters and approximately 66-72% for the digests without cell clusters). These results agree well with previous data showing that the plant cell wall is a limiting factor for the carotenoid bioaccessibility (Palmero et al*.,* 2013). It can however be suggested that also the higher viscosity in these digests can play a role, because the transfer of β-carotene to the oil droplets as well as the transfer of the enzymes to their substrates, for example lipase to oil droplets, can be hindered (McClements et al*.,* 2009). Secondly, it can be observed that the β-carotene bioaccessibility is significantly higher after the end-over-end digestion model as compared to the bioaccessibility after the periodic forces model (p-value is 0.0065) for the chromoplast fraction (from 36% to 66%) and the large cell cluster fraction (from 13% to 22%).

After the stomach phase, the most obvious difference between the two *in vitro* models was the presence of large, coalesced oil droplets after digestion using the end-over-end rotation stomach model whereas clusters of small oil droplets interspersed by surface-active compounds were observed after digestion in the stomach model with periodic forces. Although this difference in oil droplet size disappeared during the subsequent small intestinal phase, it appeared to have a

significant effect on the amount of β-carotene that was incorporated in micelles. It can thus be hypothesized that differences in oil droplet sizes during digestion are important for the β-carotene bioaccessibility. Probably this is due to the fact that the oil droplet size can not only influence the transfer of β-carotene to oil droplets, but also the interaction between lipase and the oil droplets and the transformation of oil droplets (and incorporation of β-carotene) into micelles (Borel et al*.,* 1996; Tyssandier et al*.,* 2001). Although smaller oil droplets have a larger interaction surface than large coalesced oil droplets, the bioaccessibility of the samples with larger oil droplets is higher as compared to that of the samples with smaller oil droplets (Fig. 9). Probably the surface active compounds, which are surrounding the smaller oil droplets in case of the periodic forces model (Fig. 8), hinder the lipase activity and the transformation into micelles. This effect was in particular of importance for carrot-based fractions in which the most important barrier, the plant cell wall, was absent.

The current study also shows that mixing during the *in vitro* stomach phase significantly influences the coalescence behavior of the oil droplets. In addition, viscosity influences the mixing behavior in the periodic forces model (Fig. 4), thus probably also in the end-over-end model. For example in the stomach phase with periodic forces, the flow was laminar and the shear rate is very small for the digests with large cell clusters (high viscosity), which will hinder mixing. In this case, the limiting factor can be the transfer of β-carotene to the oil droplets. An additional aspect affecting the β-carotene bioaccessibility could be the evolution of the carrot particle size during digestion. Based on the particle size distributions of the large cell clusters during digestion using the different models, it was expected that the bioaccessibility would be slightly higher when using the periodic forces digestion model (because the large cell clusters slightly broke down). The results however show that the β-carotene bioaccessibility was slightly higher when using the end-over-end digestion model. Probably, the difference in particle size reduction was negligible as compared to the effect of the viscosity and the effect of mixing on the release of the β-carotene bioaccessibility or the carrot cells were not broken down but lost some water and shrunk.

4 Conclusion

A new, simple *in vitro* stomach model in which the mechanical behavior was mimicked by an up- and downward movement was successfully implemented. The velocity field measured in this stomach model corresponds well with experimental *in vivo* and *in silico* data previously reported in literature. The stomach model was used in a two-step static *in vitro* digestion procedure and was compared with a conventionally-used, end-over-end stomach model in which the flow conditions are uncontrolled. Results showed that the *in vitro* β-carotene bioaccessibility may be dependent on a combination of factors, such as the presence of a cell wall, the viscosity of the digest and the oil droplet and plant particle size distribution, as indicated in several other studies. Besides that, this study has shown that the end-over-end digestion model and the periodic forces digestion model do not result in the same oil droplet size distribution, particle size distribution and *in vitro* β-carotene bio-accessibility. Although differences between both stomach models were observed in terms of absolute β-carotene bioaccessibility, both models (when used in combination with an end-over-end intestinal phase) seem to reveal differences in β-carotene bioaccessibility of carrot-based fractions having different barriers (the plant chromoplast structure and/or the cell wall). Therefore, conventionally-used (end-over-end rotation) digestion procedures seem appropriate to investigate such effects. Nevertheless, the results of the current study clearly show that the flow behavior in the stomach phase of *in vitro* digestion models affect the microstructural changes of plant-based foods that occur during the simulation of digestion. These differences might be of larger importance for food systems other than the ones investigated in this study or for nutritional properties other than the β-carotene bioaccessibility. Therefore, the effect of mechanical forces in the stomach phase should be more carefully studied in future research. A clear view on the exact *in vivo* flow behavior in the human stomach in this context is however imperative. The same train of thought is also applicable for the small intestinal phase of (*in vitro*) digestion which was not the focus of the current work.

Acknowledgment

This research had been financially supported by the Institute for the Promotion of Innovation through Science and Technology in Flanders (IWT-Vlaanderen). S. Van Buggenhout and R. Cardinaels are Postdoctoral Researchers funded by the Research Foundation-Flanders (FWO). T.A.J. Verrijssen is a Doctoral Researcher funded by the IWT-Vlaanderen.

References

Borel, P., Armand, M., Pasquier, B., Senft, M., Dutot, G., Melin, C., Lafont, H. & Lairon, D. (1994). Carotenoids in biological emulsions: solubility surface-to-core distribution, and release from lipid droplets. *Journal of Parenteral and Enteral Nutrition*, 18, 534-543.

Bromberg, L.E. & Barr, D.P. (2000). Self-association of mucin. *Biomacromolecules*, 1, 325-334.

Castenmiller, J.J. & West, C.E. (1998). Bioavailability and bioconversion of carotenoids. *Annual Review of Nutrition*, 18, 19-38.

Chen, J.S., Gaikwad, V., Holmes, M., Murray, B., Povey, M., Wang, Y. & Zhang, Y. (2011). Development of a simple model device for *in vitro* gastric digestion investigation. *Food and Function,* 2, 174-182.

Colle, I., Van Buggenhout, S., Van Loey, A., & Hendrickx, M. (2010). High pressure homogenization followed by thermal processing of tomato pulp: Influence on microstructure and lycopene *in vitro* bioaccessibility. *Food Research International*, 43, 2193-2200.

Courraud, J., Berger, J., Cristol, J.-P. & Avallone, S. (2013). Stability and bioaccessibility of different forms of carotenoids and vitamin A during *in vitro* digestion. *Food Chemistry,* 136, 871-877.

Dutta, D., Chaudhure, U.R. & Chakraborty, R. (2005). Structure, health benefits, antioxidant property and processing and storage of carotenoids. *African Journal of Biotechnology,* 4, 1510-1520.

Fernandez-Garcia, E., Carvajal-Lérida, I., Jarén-Galan, M., Garrido-Fernandez, J., Pérez-Galvez, A. &Hornero-Méndez, D. (2012). Carotenoids bioavailability from foods: from plant pigments to efficient

biological activities. *Food Research International,* 46, 438-450.

Ferrua, M.J. & Singh, R.P. (2010). Modeling the fluid dynamics in a human stomach to gain insight of food digestion. *Journal of Food Science*, 75, 151-162.

Hart, D.J. & Scott, K.J. (1995). Development and evaluation of an HPLC method for the analysis of carotenoids in foods, and the measurement of the carotenoid content of vegetables and fruits commonly consumed in the UK. *Food Chemistry,* 54: 101 – 111.Hedrén, E., Diaz, V. & Svanberg, U. (2002). Estimation of carotenoid accessibility from carrots determined by an *in vitro* digestion method. *European Journal of Clinical Nutrition*, 56, 425 – 430.

Hofmann, S., Rauscher, A. & Hoffmann, H. (1991). Shear induced micellar structures. *Berichte der Bunsengesellschaft für Physikalische Chemie*, 95, 153-164.

Jeffery, J., Holzenburg, A. & King, S. (2012). Physical barriers to carotenoid bioaccessibility. Ultrastructure survey of chromplast and cell wall morphology in nice carotenoid-containing fruits and vegetables. *Journal of the Science of Food and Agriculture,* 92*,* 2594-2602.

Jones, M.C., Ranger, M. & Leroux, J.C. (2003). pH-sensitive unimolecular polymeric micelles: synthesis of a novel drug carrier. *Bioconjugate Chemistry,* 14, 774-781.

Kamba, M., Seta, Y., Kusai, A., Ikeda, M. & Nishimura, K. (2000). A unique dosage form to evaluate the mechanical destructive force in the gastrointestinal tract. *International Journal of Pharmaceutics*, 208, 61-70.

Lemmens, L., Van Buggenhout, S., Van Loey, A.M. & Hendrickx, M.E. (2010). Particle size reduction leading to cell wall rupture is more important for the β-carotene bioaccessbility of raw compared to thermally processed carrots. *Journal of Agricultural and Food Chemistry*, 5, 12769-12776.

Liu, C.H. & Pine, D.J. (1996). Shear-induced gelation and fracture in micellar solutions. *Physical Review Letters*, 77, 2121-2124.

Marciani, L., Gowland, P.A., Fillery-Travis, A., Manoj, P., Wright, J., Smith, A., Young, P., Moore, R. & Spiller, R.C. (2001a). Assessment of antral grinding of a model solid meal with echo-planar imaging. *American Journal of Physiology: Gastrointestinal and Liver Physiology,* 280, 844-849.

Marciani, L., Gowland, P.A., Spiller, R.C., Manoj, P., Moore, R.J., Young, P. & Fillery-Travis, A.J. (2001b). Effect of meal viscosity and nutrients on satiety, intragastric dilution and emptying assessed by MRI. *American Journal of Physiology: Gastrointestinal and Liver Physiology,* 280, 1227-1233.

McClements, D.J., Decker, E.A. & Park, Y. (2009). Controlling lipid bioavailability through physicochemicals and structural approaches. *Critical Reviews in Food Science and Nutrition*, 49, 48-67.

Michalski, M.C., Briard, V., Desage, M. & Geloen, A. (2005). The dispersion state of milk fat influences triglyceride metabolism in the rat. A CO_2-C^{13} breath test study. *European Journal of Nutrition,* 44, 436-444.

Moelants, K.R.N., Cardinaels, R., Jolie, R.P., Verrijssen, T.A.J., Van Buggenhout, S., Zumalacarregui, L.M., Van Loey, A.M., Moldenaers, P. & Hendrickx, M.E. (2013). Relation between particle properties and rheological characteristics of carrot-derived suspensions. *Food and Bioprocess Technology,* 6, 1127-1143.

Mun, S., Decker, E. A. & McClements, D.J. (2007). Influence of emulsifier type on *in vitro* digestibility of lipid droplets by pancreatic lipase. *Food Research International,* 40, 770-781.

Pal, A., Indireshkumar, K., Schwizer, W., Abrahamsson, B., Fried, M.& Brasseur, G. (2004). Gastric flow and mixing studied using computer simulation. *Proceedings of the Royal Society London,* 271, 2587-2594.

Palafox-Carlos, H., Ayala-Zavala, J.F. & Gonzalez-Aguilar, G.A. (2011). The role of dietary fiber in the bioaccessibility and bioavailability of fruit and vegetable antioxidants. *Journal of Food Science,* 76, R6-R15.

Palmero, P., Lemmens, L., Ribas-Agusti, A., Sosa, C., Met, K., Umutoni, J.d.D., Hendrickx, M. & Van Loey, A. (2013). Novel targeted approach to better understand how natural structural barriers govern carotenoid *in vitro* bioaccessibility in vegetable-based systems. *Food Chemistry*, 141: 2036-2043.

Rosso, S. (1968). The ultrastructure of chromoplast development in red tomatoes. *Journal of Ultrastructure Research,* 25, 307-322.

Salvia-Trujillo, L., Qian, C., Martin-Belloso, O. & McClements, D.J. (2013). Influence of particle size on lipid digestion and β-carotene bioaccessibility in emulsions and nanoemulsions. *Food Chemistry,* 141, 1472-1480.

Singh, H., Yu, A. & Horne, D. (2009). Structuring food emulsions in the gastrointestinal tract to modify lipid digestion. *Progress in Lipid Research,* 48, 92-100.

Steffe, J.F. (1996). Rheological methods in food processing engineering, Freemann Press, Michigan, USA. 428 p.

Tyssandier, V., Lyan, B. & Borel, P. (2001). Main factors governing the transfer of carotenoids from emulsion lipid droplet to micelles. *Biochimica et Biophysica*, 1533, 285-292.

Vanierschot, M., Verrijssen, T.A.J., Van Buggenhout, S., Van den Bulck, E. (2013). Experimental and numerical analysis of an apparatus to apply controlled shear rates in fluid flows. . *Under consideration for publication in Chemical Engineering journal.*

Vassallo, M.J., Camilleri, M., Prather, C.M., Hanson, R.B. & Thomforde, G.M. (1992). Measurement of axial forces during emptying from the human stomach. *American Journal of Physiology,* 263, G230-G239.

Versantvoort, C.H.M., Oomen, A.G., Van de Kamp, E., Rompelberg, C.J.M. & Sips, A.J.A.M. (2005). Applicability of an *in vitro* digestion model in assessing the bioaccessibility of mycotoxins from food. *Food and Chemical Toxicology*, 43, 31-40.

Zeng, Y., Pan, Z., Ding, Y., Zhu, A., Cao, H., Xu, Q. & Deng, X. (2011). A proteomic analysis of the chromoplasts isolated from sweet orange fruits (*Citrus sinensis* (L.) Osbeck). *Journal of Experimental Botany,* 62, 5297-5309.

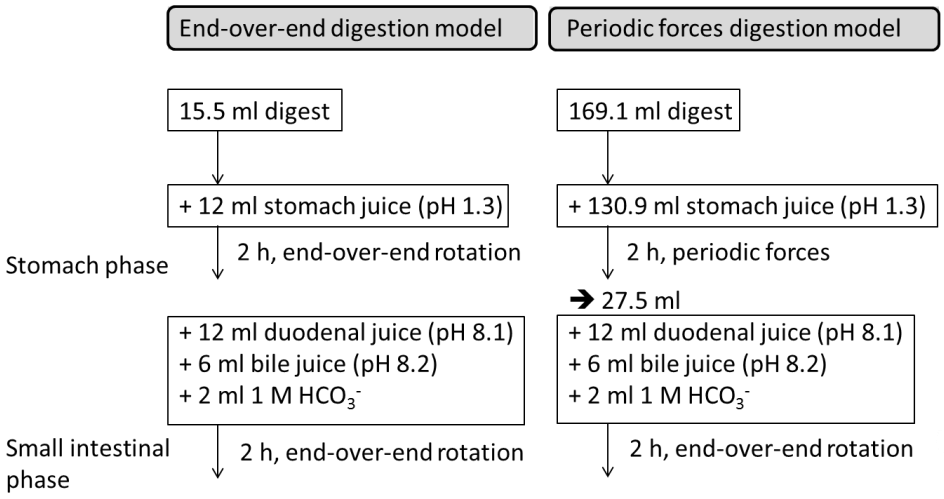

Figure 1: Schematic overview of the two *in vitro* digestion models. The stomach, duodenal and bile juices are composed according to the method of Versantvoort et al. (2005).

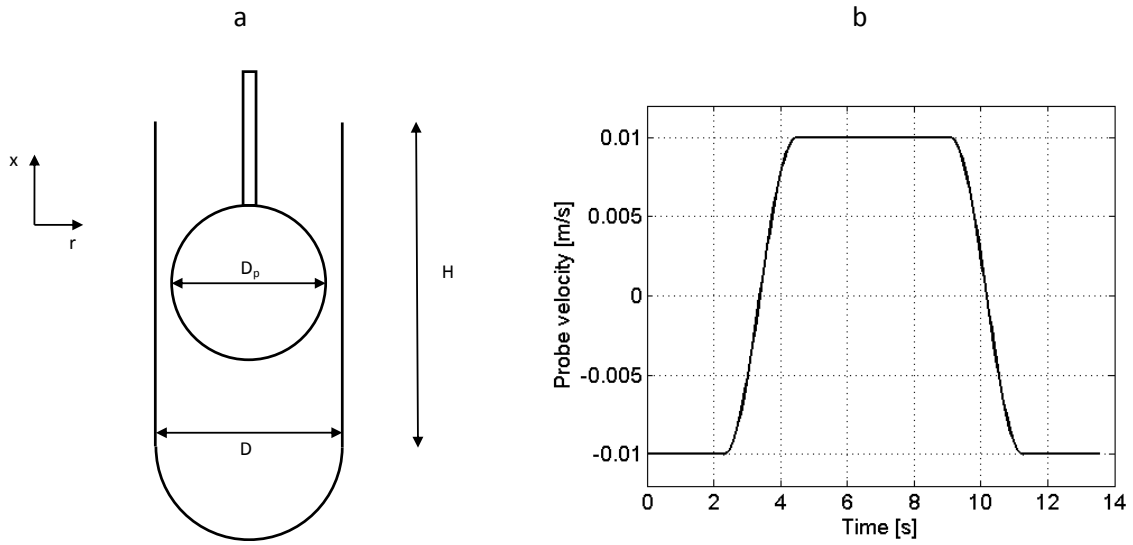

Figure 2: (a) Schematic view of the *in vitro* periodic forces stomach model (with D = internal diameter, H = internal height, Dp = diameter of the spherical teflon probe); (b) Velocity of the probe versus time.

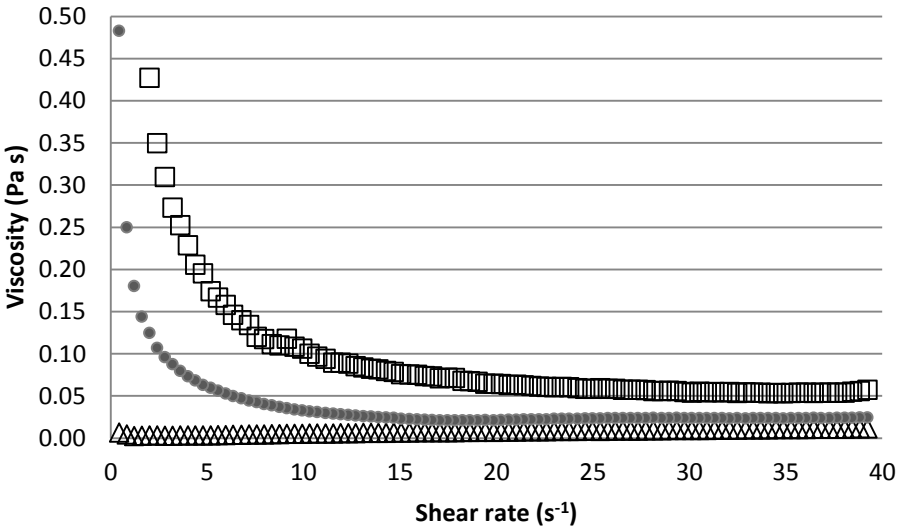

Figure 3: Non-Newtonian behavior for different digests (enriched oil emulsion or chromoplasts (Δ), small cell clusters (•)and large cell clusters(□)) with stomach juices.

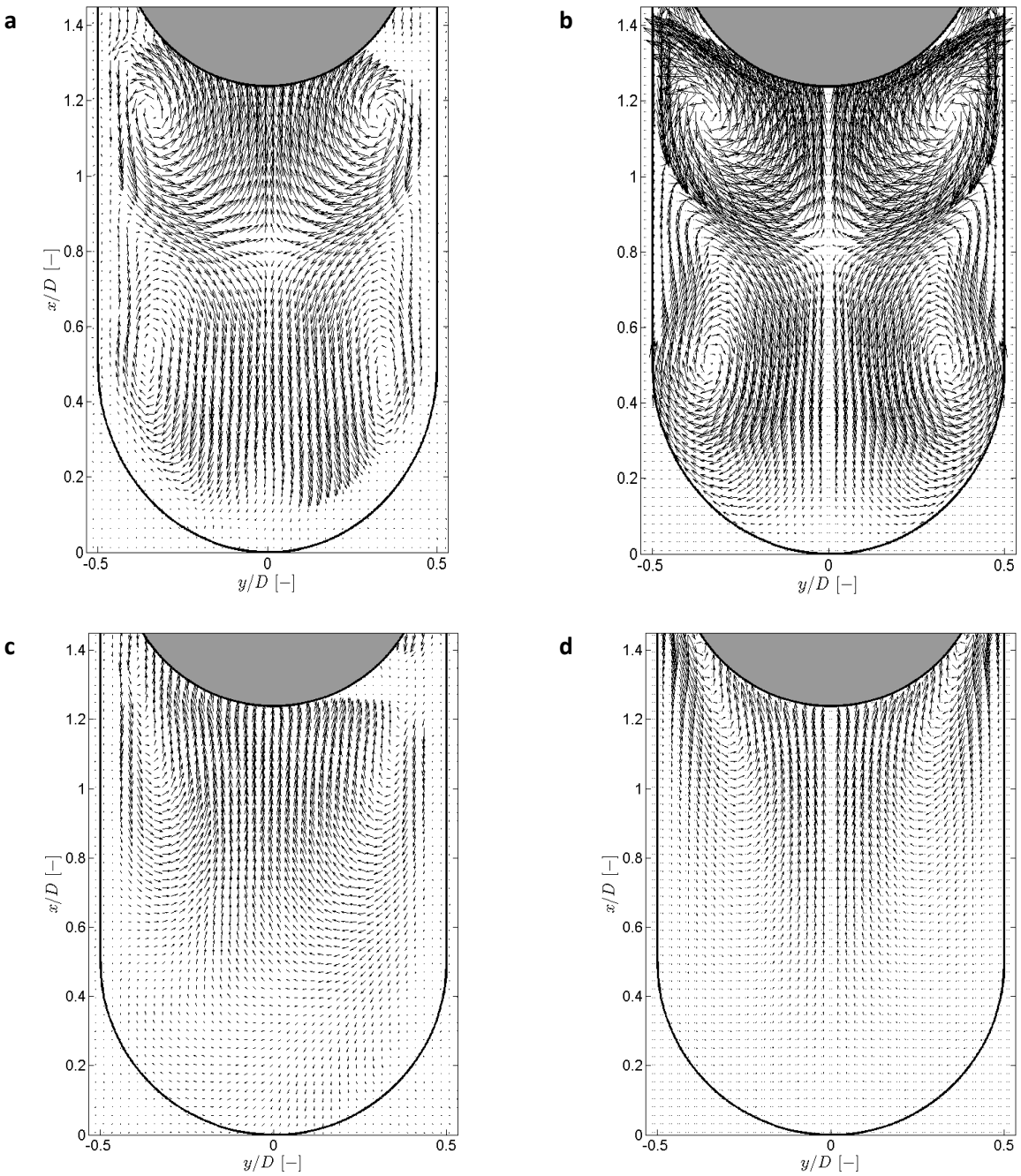

Figure 4: Velocity vectors of the flow field inside the *in vitro* setup for a low viscosity fluid (μ=1 mPa.s) (a,b) and for a higher viscosity fluid (μ=12 mPa.s) (c,d). PIV measurements (a, c) are compared with CFD simulations (b,d) (probe on maximal height).

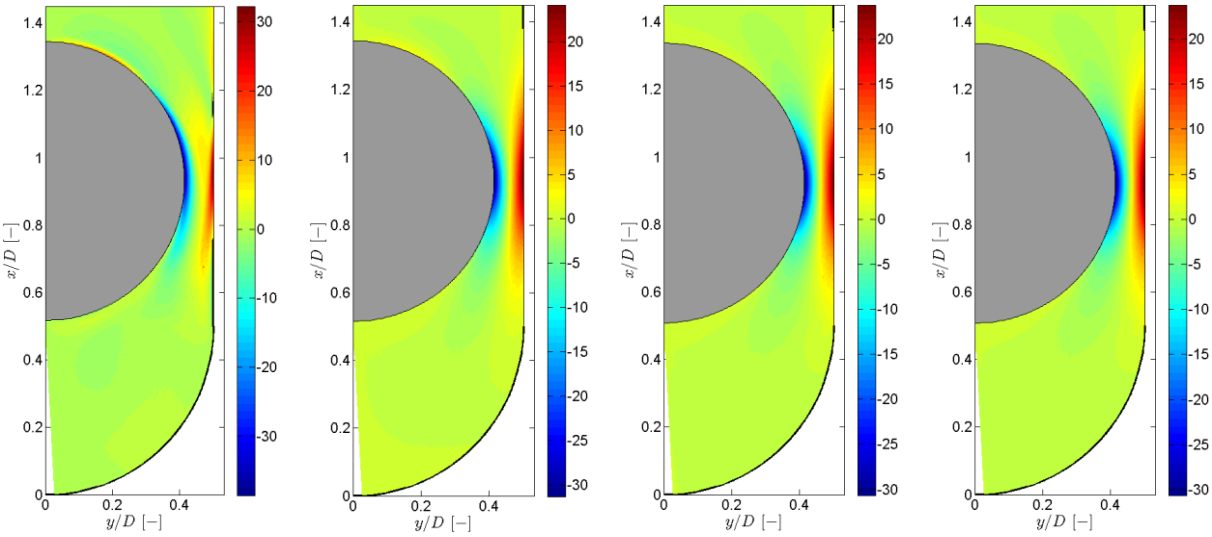

Figure 5: Shear rates [s^{-1}] of the flow field for various viscosities. From left to right: 1 mPa.s, 12 mPa.s, 50 mPa.s and 80 mPa.s

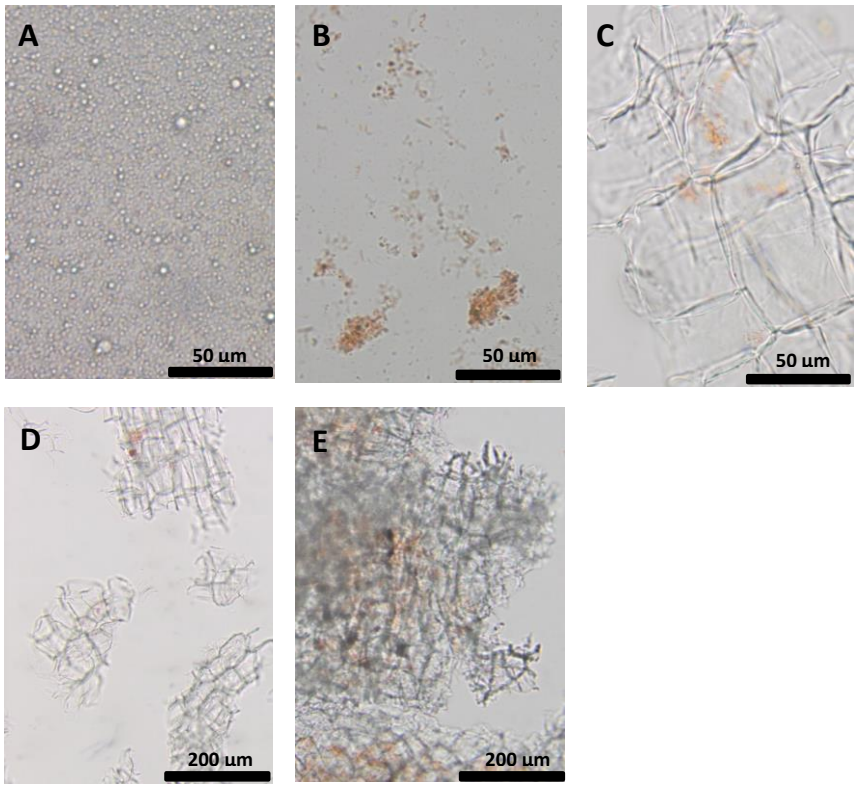

Figure 6: Representative microscopic images of (a) the enriched oil emulsion fraction (40x), (b) the chromoplast fraction (40x), (c) the cell cluster fractions (40x), (d) the small cell cluster fraction (10x) and (e) the large cell cluster fraction (10x) (before digestion).

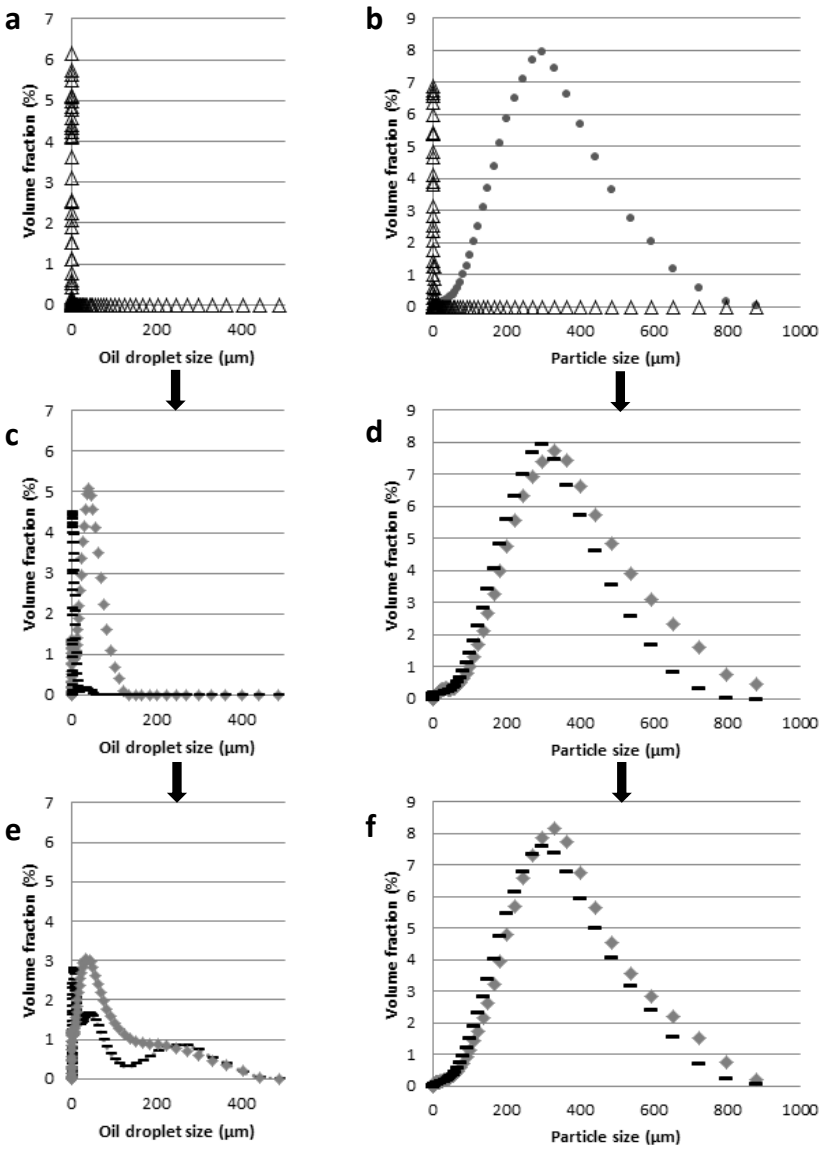

Figure 7: Oil droplet and particle size distributions of the oil emulsion (Δ) (a-c-e) and the small cell cluster fraction (•) (b-d-f) (where to oil emulsion (Δ) was added (Table 1)) during digestion (a,b: before digestion; c,d: after the stomach phase; e,f: after the small intestinal phase), obtained using different digestion models, namely the end-over-end model ( ) or the periodic forces model (—)

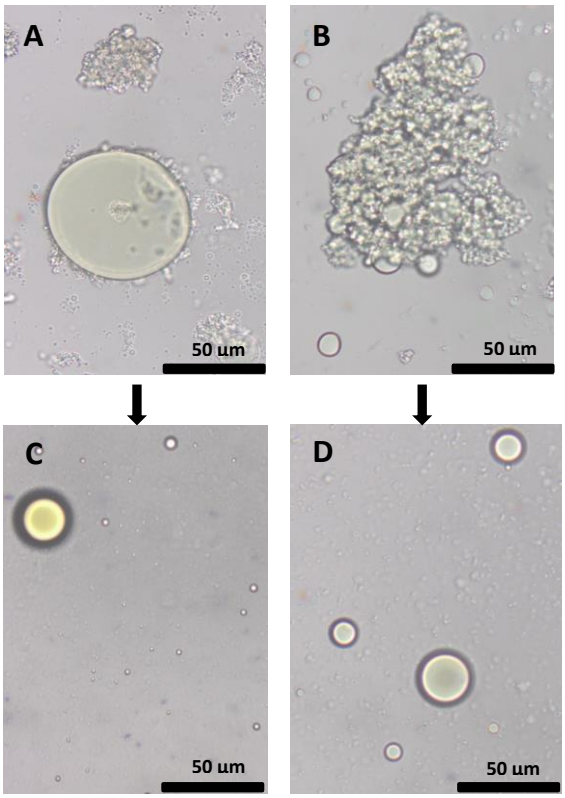

Figure 8: Representative microscopic images of the oil droplet distributions in the enriched oil emulsion fraction (a) after the end-over-end stomach phase (10x), (c) after end-over-end digestion model (10x), (b) after periodic forces stomach phase (10x) and (d) after periodic forces digestion model (10x)

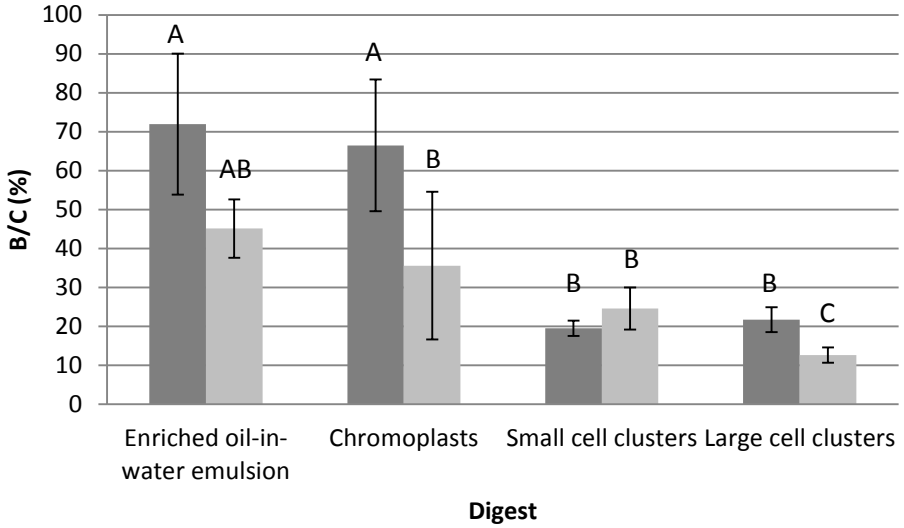

Figure 9: Percentage *in vitro* β-carotene bioaccessibility (calculated as the absolute β-carotene bioaccessibility of a particular fraction (B) divided by the initial β-carotene concentration (C)) (mean ± standard deviation) in the different

digests after the end-over-end digestion model (■) or the periodic forces digestion model (■). Significant differences (Tukey test: $P<0.05$) are indicated with different letters (A, B, C).